Spatially resolved transcriptomics reveals plant host responses to pathogens

Michael Giolai[1,2], Walter Verweij[2,3], Ashleigh Lister[2], Darren Heavens[2], Iain Macaulay[2] and Matthew D. Clark[2,4 *]

[1] John Innes Centre, Norwich Research Park, Norwich, UK

[2] Earlham Institute, Norwich Research Park, Norwich, UK

[3] Enza Zaden, Enkhuizen, NL

[4] Natural History Museum, London, UK

Address correspondence to Matthew Clark, Natural History Museum, London, UK; E-mail: matt.clark@nhm.ac.uk

Abstract

Background: Thorough understanding of complex model systems requires the characterisation of processes in different cell types of an organism. This can be achieved with high-throughput spatial transcriptomics at a large scale. However, for plant model systems this is still challenging as suitable transcriptomics methods are sparsely available. Here we present Grid-seq, an easy to adopt, micro-scale spatial-transcriptomics workflow that allows to study expression profiles across small areas of plant tissue at a fraction of the cost of existing sequencing-based methods.

Results: We compare the Grid-seq method with widely used library preparation methods (Illumina TruSeq). In spatial experiments we show that the Grid-seq method is sensitive enough to identify expression differences across a plant organ. We further assess the spatial transcriptome response of *Arabidopsis thaliana* leaves exposed to the bacterial molecule flagellin-22.

Conclusion: We show that our method can be used to identify known, rapidly flagellin-22 elicited genes, plant immune response pathways to bacterial attack and spatial expression patterns of genes associated with these pathways.

Key words:

Spatial transcriptomics, transcriptomics, transcriptome landscape, RNA-seq, plant immunity, plant defence response, flg22, biotic interaction, Grid-seq

Background

Most model plants and all crops species are multicellular, consisting of multiple organs and cell types with a multitude of physiological states [1]. A thorough understanding of these complex systems requires the ability to dissect and characterise processes in the different organs and cell types. This is challenging, though recently multi-omics single-cell studies have been flourishing [2], but high-throughput, high-resolution methodologies that assess molecular conditions with spatial resolution are sparsely available [3–6].

Although some spatial and low-input transcriptome profiling methods have been developed for animal model organisms [3–5,7], these methods are difficult to transfer to plants [6,8]. In comparison to animal cells, plant tissues hold a series of additional challenges: the robust plant cell wall requires specialised sample preparation (which makes reproducible, high-throughput sample preparation more difficult) and some plant secondary metabolites e.g. polyphenols can inhibit downstream enzymatic processes [9].For plants, single plant cells (protoplasts) can be obtained by enzymatic removal of plant-cell walls and subsequent fluorescent activated cell sorting (FACS) assays [10]. At the sub-cellular scale plant nuclei can be isolated within minutes by cell lysis and FACS [10–12]. However, 'stimulus and response' assays, such as differential gene-expression experiments or the characterisation of cell-type transcripts could be affected by these additional experimental procedures before RNA-extraction. Another important factor is the loss of spatial information when nuclei or protoplasts are extracted from a tissue. Thus methods such as fluorescent in-situ hybridisation (FISH) [13], laser-capture microdissection (LCM) [14–16] or the SPATiAL TRANSCRIPTOMICS [4,6] workflow are better suited to understand spatial transcription changes. However, all three methods need specific tissue preparations (e.g. cryo-sectioning, permeabilization

49 or fixation) and specialised protocols to assess transcriptome levels: FISH methods require imaging of
50 transcripts and are restricted to multiplexing a few fluorescent anti-sense probes at a time [3], LCM
51 requires specialised equipment and training for precise, laborious excision of specific tissue elements
52 [6] and the SPATiAL TRANSCRIPTOMICS protocol requires preparation of thinly sectioned,
53 permeabilised samples and custom made DNA arrays [4,6].

54 Despite the high level of resolution that can be achieved with all these methods, they are not easily
55 applied in most laboratories. We aimed to overcome this with our Grid-seq workflow. Grid-seq is
56 designed to quickly process mechanically dissected samples into sequencing libraries using standard
57 laboratory equipment and can be used in most modern laboratories. Grid-seq is based on three
58 consecutive steps: (1) rapid, mechanical sample dissection of small e.g. 1 mm^2 leaf areas, (2) a high-
59 throughput method for high quality mRNA extraction of difficult to lyse plant tissues and (3) next
60 generation sequencing (NGS) library construction (**Figure 1**).

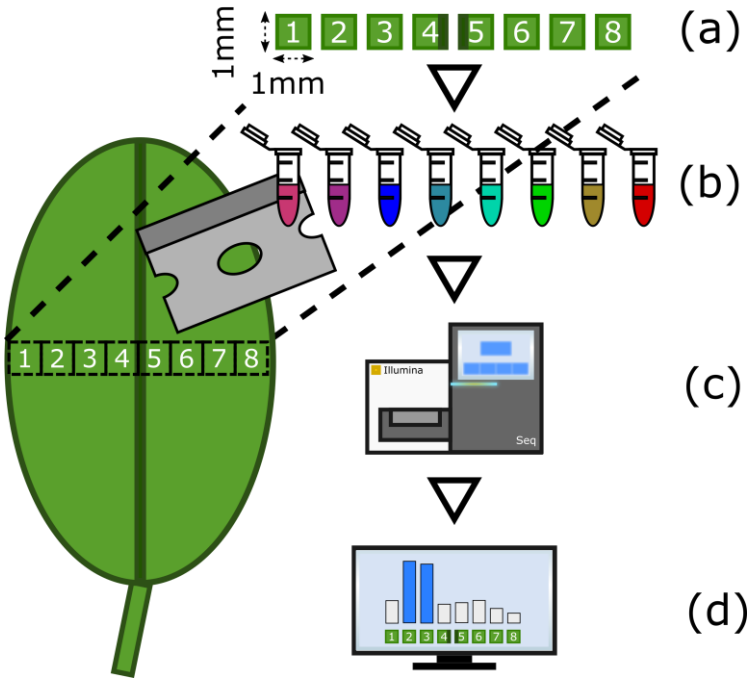

61

62 **Figure 1 Overview of the Grid-seq workflow:** (a) Tissue sections of approximately 1 mm^2 size are mechanically extracted
63 (e.g. a cross-section of a leaf) and after mRNA extraction (b) prepared into uniquely barcoded Illumina sequencing libraries.
64 After (c) Illumina sequencing (d) transcript specific, spatial expression data can be assessed and analysed.

65 In a series of experiments, we compare the performance of Grid-seq with standard RNA-seq (Illumina
66 TruSeq) experiments. Using Illumina sequencing we identify differentially expressed (DE) genes in 1D
67 (across lateral leaf sections) observing how transcripts and expression levels vary across the tissues
68 that make up the leaf organ. We compare large-scale vs. fine-scale transcriptome experiments ability
69 to detect plant responses induced by the bacterial peptide flagellin-22 (flg22), a well-described
70 pathogen-associated molecular pattern (PAMP) that triggers plant immune responses [17]. By
71 comparing our data with published datasets for 'flagellin rapidly elicited' (FLARE) genes [18] we
72 identified 143 of 253 described FLARE genes that overlap with our data, and a further 428 genes with
73 similar expression patterns to FLARE genes. We show that the detected 428 transcripts, are enriched
74 for plant defence responses and that spatial transcriptome data can be used to reconstruct the
75 spatial expression of pathway components across leaves. In additional pilot experiments using
76 *Arabidopsis thaliana* and the oomycete pathogen *Albugo laibachii* we also show that the dual dataset
77 of both host and pathogen, are captured, and spatial expression profiles can be constructed which
78 could be used to study the biotic interactions in infections

79 **Results**

80 **Does leaf dissection induce wounding response gene expression profiles?**

81 Physical wounding of plants is known to induce wounding related gene expression [19]. This is an
82 important point to consider as the Grid-seq workflow dissects tissue into ~ 1 mm^2 squares followed
83 by immediate snap freezing on dry ice. Yet dissection could potentially lead to activation of wounding
84 related gene expression and dissection takes longer as the resolution increases (grid size). As any
85 wounding effect could form a technical limitation to Grid-seq we measured the number of DE-genes
86 found after tissue dissection. For this we prepared ~1 mm^2 leaf squares (3 biological replicates per
87 time-point) at the time-points: 0-minutes, 2.5-minutes, 5-minutes and 10-minutes between cutting
88 and freezing on dry ice (when all enzymatic reactions cease). To determine the number of DE-genes
89 at each time-point we compared the 2.5-minute, 5-minute and 10-minute samples with the 0-minute

90 samples as an unwounded reference. This analysis showed just 1 DE-gene (AT2G37130) at the 2.5-
91 minute time-point (which was not significant at later time-points) there were no DE-genes at the 5-
92 minute time-point and 13 genes at the 10-minute time-point (see: **Additional_file1.docx** and
93 **Additional_file2.xlsx**) suggesting that the transcriptional response to wounding starts between 5 and
94 10 minutes. We looked for enriched biological processes in the combined set of 14 genes and
95 detected three genes at the 10-minute time-point being associated with the GO-term 'response to
96 wounding': *TPS04, TAT3* and AT1G62660 (see: **Additional_file1.docx** and **Additional_file2.xlsx**). This
97 indicates that it is highly desirable to cut and snap freeze sample material within 10 minutes to avoid
98 perturbation of results – a time window in which we find that sample dissection is easily achievable.

99 **Spatially resolved transcriptomics data reveals leaf tissue specific gene expression**

100 We assayed Grid-seq's ability to detect known gene expression differences between tissue types in
101 untreated leaves. Briefly, we dissected a lateral cross-section of an *A. thaliana* leaf (3 biological
102 replicates) into a 1-dimensional (1D) expression map of eight circa1 mm^2 squares (**Figure *2*A**)**.** Each
103 cross-section was sampled according to the same pattern: the leaf margins were located at square-1
104 and square-8 and the midvein at square-5. We then identified DE-genes by comparing the midvein
105 with the lamina and the leaf margins with the lamina. This resulted in 393 DE-genes for the midvein
106 and 686 DE-genes for the leaf margins comparison (**Figure 2** and file: **Additional_file2.xlsx**).

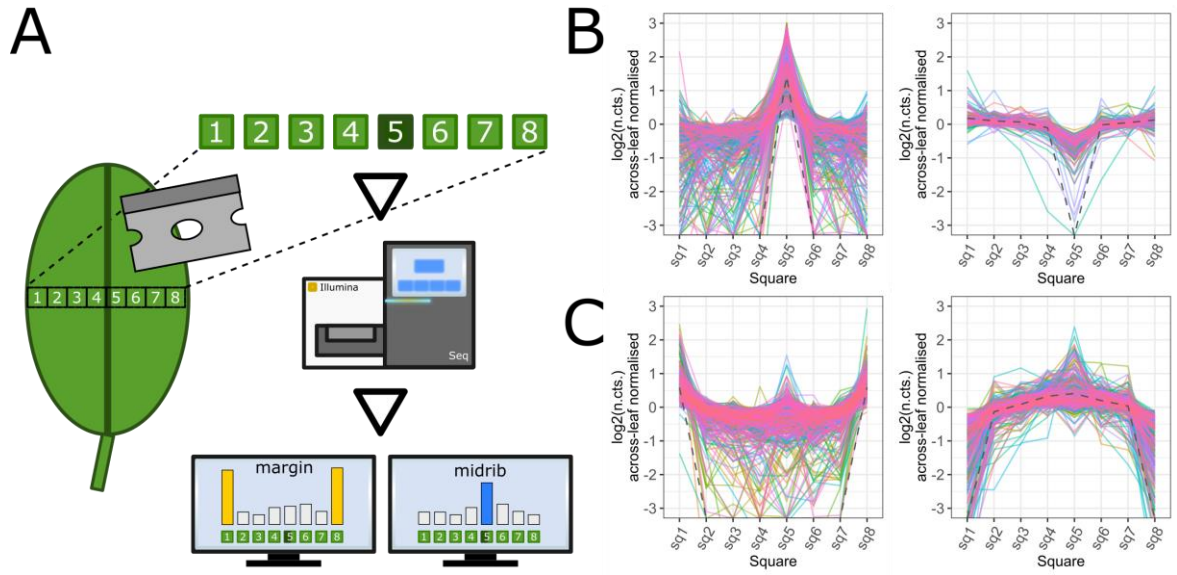

Figure 2 Identification of midvein and edge DE-genes in a lateral 1D leaf cross-section: (A) DE-gene analysis of a 1D *A. thaliana* leaf lateral cross sections by comparing the midvein (square-5) or the margin squares (square-1 and square-8) with the 'bulk' (remaining) leaf sections. The two images in (B) show 393 DE-genes with higher (left, 256 DE genes) or lower (right, 137 DE genes) expression values in the midvein. The images in (C) show 686 DE-genes higher (left, 403 DE genes) or lower (right, 283 DE genes) expression in the leaf margins. The grey dashed line in each plot (B and C) represents a trend-line for the average log2(counts) of all genes normalised across the leaf squares.

Comparison of spatial and bulk transcriptomics after localised flg22 stimulation

To compare spatial (only treated areas) with bulk (large leaf areas with treated and untreated areas) PAMP immune responses we used a flg-22 syringe infiltration assay. For this we produced small, local infiltration spots on the abaxial, left-hand side of a leaf of 6 biological *A. thaliana* replicates using either 500 nM flg22 or water (**Figure 3A**). We incubated the plants for 1 hour and sampled by dissecting leaf samples with a 1D system as above, briefly: square-1 (in the middle of the left half of a leaf) as infiltration spot and then laterally towards the midvein square-2 as non-vascular leaf tissue, square-3 as the midvein and square-4 as non-vascular leaf tissue.

In our analysis we wanted to measure how bulk RNA-seq datasets compared to spatially collected ones by using the number of detectable DE-genes. We hypothesised that the spatial analysis of the small, local treatment spot (square-1) and its surroundings (square-2, square-3 and square-4) would reveal more and distinct types (or waves) of flg22 responsive DE-genes than a bulk analysis would –

especially of rarer transcripts. To measure the effect of spatial information alone we simulated an *in silico* flg22 bulk experiment by combining the data from flg22 or water treated square-1 with the other untreated squares-2, 3 and 4 of the same leaf. We then called the treatment responsive DE-genes from the bulk files, detecting 65 DE-genes (39 higher expressed, 26 lower expressed) 1 hour after flg22 infiltration. We detected 887 more DE-genes (952 in total) by comparing the single squares of the flg22 and water infiltration dataset: 646 DE-genes for square-1 (416 higher, 230 lower expressed), 401 DE-genes for square-2 (306 higher, 95 lower expressed), 9 DE-genes for square-3 (8 higher, 1 lower expressed) and any DE-genes for square-4 (see: **Additional_file2.xlsx**). In contrast comparing the gene lists of the *in silico* bulk and spatial analysis we detected that 4 DE-genes were exclusively called from the bulk dataset and 64 genes were shared by both datasets.

To identify the biological processes uncovered by our transcriptomics experiments we performed a GO-term enrichment analysis the spatial flg22 related DE-gene datasets. From all (952) DE-genes we obtained 168 enriched GO-terms; among them we observed a high number of biological processes related to stress and defence responses (see: **Figure 3B**).

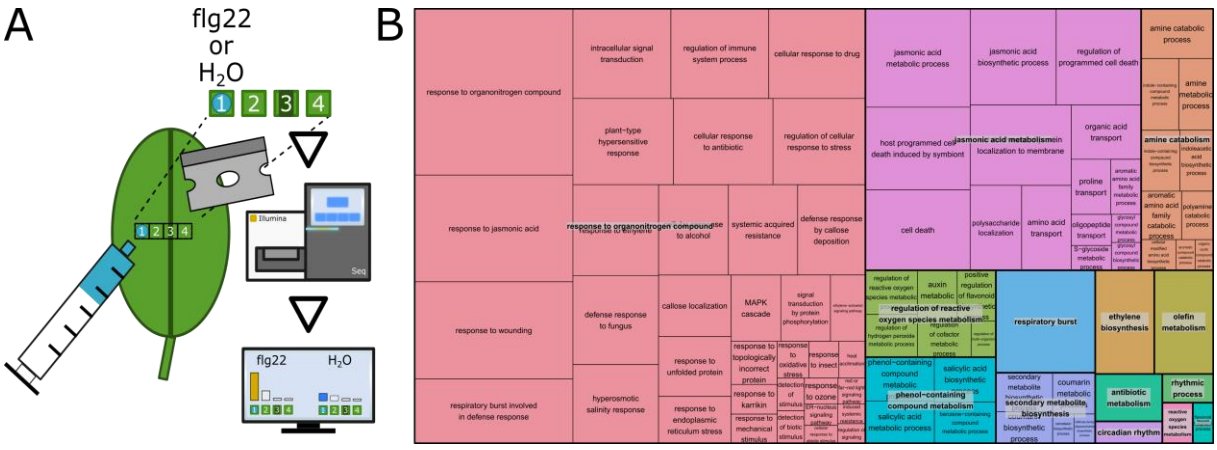

Figure 3 Elicitation of early *A. thaliana* defence response genes by infiltrating the bacterial peptide flg22: (A) To provide a strong stress stimulus we used syringe infiltration of either 500 nM flg22 or, as a control, water on a small area of the abaxial side of a leaf (square-1). 1 hour after infiltration we dissected 4 squares of a lateral leaf section with square-1 being the infiltration spot, square-2 and square-4 untreated, non-vascular leaf tissue and square-3 as midvein. The figure in (B) shows the REVIGO *[20]* treemap of the detected 168 GO-terms grouped under parent terms such as 'response to organonitrogen compound' (rose), 'jasmonic acid metabolism' (purple), 'amine catabolism' (orange) 'regulation of reactive

147 oxygen species metabolism' (green), 'phenol-containing compound metabolism' (azure blue), 'respiratory burst' (blue), etc..
148 The size of each rectangle relates to the absolute log10(q-value) – the larger the more significant.

149 **Early elicited flg22 response genes of local, fine-scale stimulation**

150 To simulate an initial pathogen encounter we used a milder stimulus method than the above
151 described syringe infiltration: we prepared 6 biological *A. thaliana* replicates by depositing 1 µl of 500
152 nM flg22 on square-3 of the abaxial side of a leaf and 1 µl of water (internal control) on square-6
153 (equivalent locations due to leaf bilateral symmetry). After one hour we extracted the treated leaf
154 area as a 1D lateral cross-section containing 8 separate 1 mm^2 squares (**Figure 4A**). We were
155 interested in DE-genes at the site of flg22 spotting (square-3) and in adjacent sections (square-2 and
156 square-4) as we reasoned that the plant would respond to the PAMP locally at first and then
157 responses via signalling to adjacent tissues and the rest of the plant. We called DE-genes by
158 comparing the flg22 with the water droplet spots (square-3 vs square-6) and the adjacent sections
159 with their corresponding bilateral equivalents (square-2 vs square-7 and square-4 vs square-5). Due
160 to the milder stimulus in comparison to the flg22 infiltration dataset we expected the number of DE-
161 genes could be lower than in the syringe infiltration experiment where we detected 952 DE genes.
162 Indeed, we identified a lower number of 523 DE-genes (491 higher expressed, 32 lower expressed)
163 for the droplet spot, and 5 DE-genes in the adjacent sections (1 higher expressed DE-gene in the
164 square-4 square-5 comparison and 4 higher expressed DE-genes in the square-2 vs square 7
165 comparison). Thus, in total we detected 526 individual DE-genes.

166 We compared both droplet spotting and syringe infiltration datasets (each dataset was collected 1
167 hour after flg22 exposure) for biological processes using GO-term enrichment. Both experiments
168 produced a similar number of enriched GO-terms with 159 biological processes enriched in the
169 droplet spotting dataset and 168 biological processes enriched in the infiltration dataset, with an
170 overlap of 132 biological processes (83.0 % of the spotting dataset and 78.5 % of the infiltration
171 dataset) between both datasets (see: **Additional_file2.xlsx**). The percentage of shared, enriched GO-

172 terms indicated the presence of a similar plant response to flg22 in both experiments despite the
173 difference in stimulus strength.

174 We measured the DE-genes with the 253 flagellin rapidly elicited (FLARE) genes described by seedling
175 and cell culture flg22 exposure experiment of Navarro et al. [18] (see: **Additional_file2.xlsx**). We
176 found that the DE-genes of the droplet spotting experiment contained 24.90 % FLARE genes (63 of
177 253 genes). These consisted of 32 FLARE genes associated with signal transduction, 11 genes
178 associated with roles in signal perception, 14 with known or putative roles as effector proteins and 9
179 FLARE genes identified by Navarro et al. as 'other' FLAREs (see: **Additional_file2.xlsx**). We found a
180 slightly higher number in the infiltration experiment: 80 DE genes were shared with the 253 FLARE
181 genes (31.62 %) with 39 genes associated with signal transduction, 16 genes in signal perception, 15
182 genes with known or putative roles as effector proteins and 11 genes with other functions (see:
183 **Additional_file2.xlsx**). Interestingly the % of known FLARE and the number of enriched biological
184 processes was higher in the infiltration than the spotting experiment (possibly suggesting other
185 processes are triggered by infiltration).

186 We were interested in the spatial expression patterns of the 63 shared FLARE genes between our
187 droplet spotting experiment and the Navarro et al. dataset. For this we visualised the expression
188 patterns of the FLAREs across the studied leaf area. All 63 FLARE genes showed high expression levels
189 at the area of flg22 exposure in comparison to adjacent leaf squares (Figure 5**B**). To study the
190 expression profiles of the remaining 460 DE genes identified in the flg22 droplet spotting experiment,
191 we affinity propagation clustered [21] these DE genes based on their spatial expression patterns and
192 visualised the expression profile of each cluster (**Figure 4C**). We identified three gene clusters: two of
193 the three clusters contained genes with higher expression levels at or adjacent to the area of flg22
194 treatment and one cluster contained a group of lower expressed genes at the flg22 treated area
195 (**Figure 4C**).

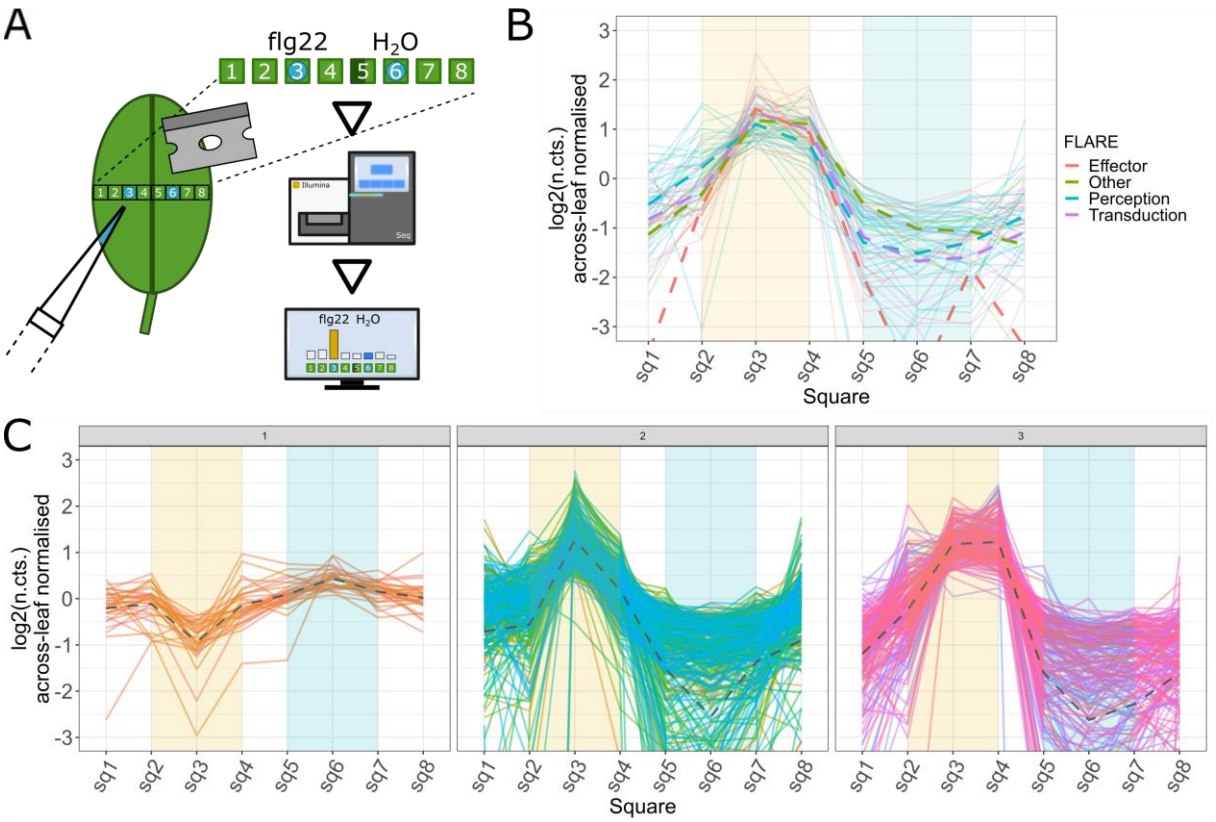

Figure 4 Elicitation of early *A. thaliana* defence response genes by droplet depositing the bacterial peptide flg22: (A) As a milder stress stimulus than flg22 syringe infiltration we pipetted a 1 µl droplet of 500 nM flg22 and, as an internal control, water on the abaxial surface of a leaf. 1 hour after droplet deposition we dissected a lateral section into 8 squares with square-1 and square-8 as leaf margins, square-3 as flg22 treated spot, square-6 as water treated spot and square-5 as midvein. Image (B) shows an overlay of the spatial expression patterns of the 63 FLARE genes characterised by Navarro et al. *[18]* present in our dataset. Each group is coloured separately, the average expression of each FLARE group is shown as the dashed line. Image (C) shows the spatial expression of all 523 detected DE genes grouped in three different clusters. From left to right: One cluster (1) contains genes which are lower expressed at the flg22 treatment area, two clusters contain genes with higher expression at the flg22 treatment spot in comparison to adjacent areas but with narrower (2) and broader (3) spatial expression. The yellow background in the plot indicates the flg22 treated area, the blue background indicates the water treated control area.

We analysed all clusters for enriched biological processes using GO-term analysis. We could not detect any enrichment in biological processes for the cluster containing the DE genes which were lower expressed at the flg22 site. The two clusters with expression peaks at the site of flg22 stimulation however enriched 135 and 122 biological processes. Of all biological processes 100 were shared between both clusters and 35 as well as 22 biological processes unique for each cluster

respectively (see: **Additional_file1.docx** and **Additional_file2.xlsx**). This suggests that biological processes (host responses) could be associated with the spatial expression profiles of their corresponding genes. To study this further we used the affinity propagation clustering algorithm [21] to determine the number of clusters without a specified cluster number preference value. This grouped the 523 DE genes into 36 more tightly resolved spatial expression clusters, comprising 35 clusters with between three and 57 genes and a single cluster containing only one gene (**Figure 5A**). 28 of 35 clusters were enriched for biological processes (see: **Additional_file3.csv**). To test if different spatial expression patterns enrich different biological processes, we correlated all multi-gene clusters based on the presence / absence of all enriched GO-terms. We saw little overlap in biological processes between clusters, indicating that each spatial expression cluster enriched slightly different GO-terms. (**Figure 5B** and **Additional_file3.csv**).

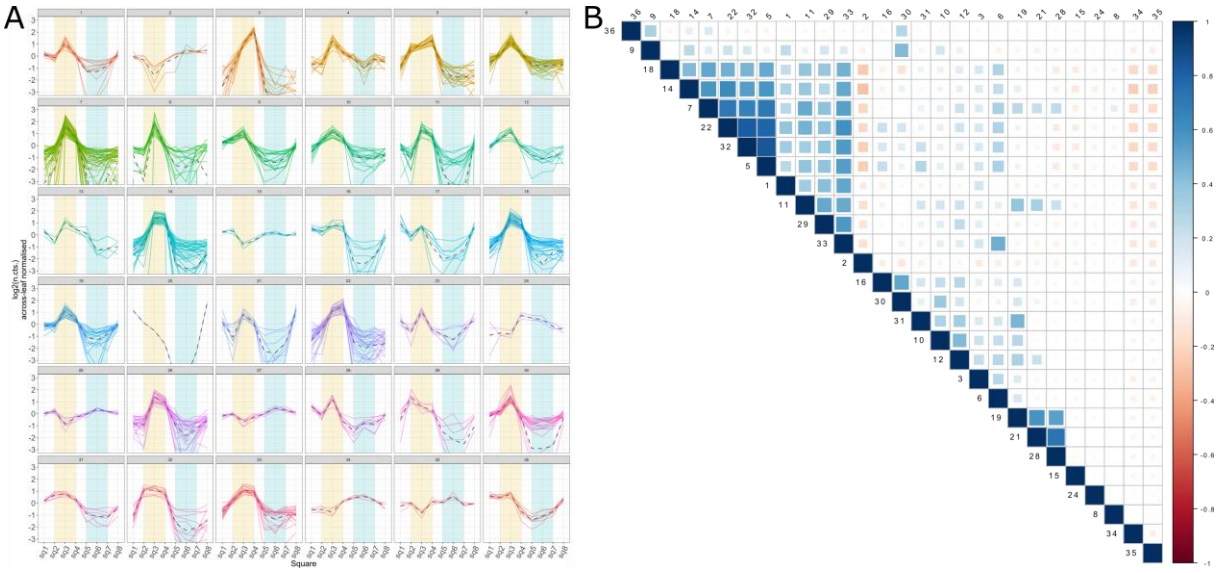

Figure 5 Unsupervised clustering of flg22 elicited DE genes and GO-term correlation matrix of the predicted clusters: Figure (A) shows the expression profiles of the 523 flg22 elicited DE genes grouped to 36 clusters precisely clustered according to their spatial expression pattern across the tested leaf area. Many of the clusters show differences in their induction profile at the site of flg22 deposition (yellow background) but also differences in expression at the water treated area (blue background) or the expression at the leaf boarders. Figure (B) shows the correlation analysis of the enriched GO-terms from the genes of the spatial clusters shown in (A) – 28 clusters grouped with hierarchical clustering for enriched GO-terms.

233 **Characterisation of spatial regulatory elements**

234 We characterised the expression patterns of the 36 obtained clusters in **Figure 5**. 11 clusters (1, 2, 6,
235 8, 12, 15, 23, 25, 28, 30, 35) showed a peak of higher expression at the site of flg22 perception. 14
236 clusters (3, 5, 7, 10, 11, 14, 18, 19, 21, 22, 26, 29, 32, 33) indicated spatially elevated gene expression
237 patterns with higher expression also at sites adjacent to the area of flg22 perception. The remaining
238 11 clusters showed less clear expression profiles (**Additional_file2.xlsx**).

239 To identify plant regulatory elements that are potentially involved in PAMP perception and signal
240 propagation to adjacent areas, we selected DE genes belonging to the flg22 locally and adjacently
241 elevated clusters, and then filtered the genes for the TAIR-10 [22] GO-terms 'receptor' and
242 'transcription'. This included the leucine-rich repeat receptor like kinase (LRR-RLK) *RLK7* (cluster 1)
243 which was locally elevated, whereas the LRR-RLK *CERK1* and the serine/threonine-protein kinase
244 *PSKR1* while strongly elevated at the area of flg22 perception were also broadly expressed
245 throughout all sites (cluster 7). We detected a larger set of 48 DE genes associated with
246 transcriptional processes. WRKY (15 genes), ERF (8 genes) and MYB (4 genes) transcription factor
247 family members [23–25] were the most abundant in our dataset.

248 To start to understand the possible gene regulatory network controlling this spatial expression we
249 used the TF2Network software [26] to search for putative regulatory interactions between these 48
250 DE genes i.e. by transcription factor binding. The resulting gene networks are built from genes with
251 at least one target and a q-value < 0.01 (see **Additional_file1.docx**). These linked 4 transcription
252 factors of which all belonged to the WRKY family (*WRKY11*, *WRKY15*, *WRKY17* and *WRKY47)* to 388
253 other DE genes indicating a possible regulatory network (TF2Network authors suggest their tools has
254 a very low false positive rate, whilst being sensitive enough to detect 75-92% of correct links).

255 Of the detected transcription factors *WRKY17* (cluster 4) and *WRKY47* (cluster 8) were associated
256 with local expression patterns, whereas *WRKY11* (cluster 10) and *WRKY15* (cluster 10) showed
257 spatially wider expression.

258 **Discussion**

259 The ability to profile gene expression patterns in small specific areas without bulk sequencing
260 provides access to lower level transcripts, especially tissue and cell specific ones [3–5,28–30]. Spatial,
261 low RNA-input transcriptomics methods allow deeper insights in how an organism develops and
262 reacts to its environment than conventional "gross-scale" RNA-seq methods [4–6]. By combining
263 rapid dissection with Grid-seq, we were able to reconstruct spatial transcriptional differences across
264 organs and localised defence responses.

265 Although some specialised protocols are already available to profile transcriptomes from minute
266 input amounts such as single-cells [2,10], or even nuclei [11,12], these detailed techniques do not
267 retain the spatial information of a starting tissue and any time-consuming experimental procedures
268 to preserve spatial data could induce experimental bias by altering the transcriptome. For spatial
269 analyses in plants LCM [14,15] methods for fine-scale transcriptome analyses are available, however,
270 these procedures are time-consuming and this limits the scale of the application. Large scale spatial
271 analysis have been performed in the past [8], but still required bulk sampling of material by pooling
272 multiple replicates. Methods relying on sample dissection and reaction-tube processing of tissue
273 sections to sequencing libraries have already proven to be able to identify transcripts patterns in the
274 zebrafish embryo [5] allowing to process multiple samples easily for modelling the transcriptome
275 landscape of an entire organism. Recently Giacomello et al. [6] published a workflow to blot the
276 transcriptome landscape from permeabilised plant tissues by vertical diffusion onto a slide
277 containing an array of barcoded primers and on slide library construction which maintained the
278 mRNA's location via the barcode. This method, for the first time in plants, allowed access to spatial
279 transcriptome data in thin tissue slices of plant organs with a great level of resolution. However,
280 gathering and optimisation of permeabilization conditions of thin tissue sections can be challenging
281 especially if the tissue due to the volume and shape of the sample, are not suitable to be processed
282 on an array and the workflow is only commercially accessible.

283 Plants grow in a microbiologically rich environment with their own microbiomes and even symbionts
284 [31], but they are also attacked by pathogens, pests, herbivores and other biotic stresses [32]. As
285 plants can't move away from attacks they defend themselves using molecular and cellular biology
286 responses, however overstimulation of these processes leads to stunted development and lower
287 fitness [17]. As plants must balance the need to defend themselves against constant plant-microbial
288 interactions and attack [17] we hypothesised that local attacks might be integrated into a plant-wide
289 defence response decision. Yet there are no appropriate assays to measure the molecular and cell
290 biology changes at the required resolution. Here, we demonstrate a novel micro-scale method to
291 pursue spatial transcriptomics experiments in plants in an easy manner based on easily accessible
292 methods in sequencing library construction and bioinformatics tools.

293 We developed a robust micro-spatial expression methodology that enables the creation of
294 transcriptome level maps from very small amounts of any eukaryotic tissue. The Grid-seq workflow
295 evolved by transferring elements from existing single-cell RNA-seq methods [33,34] from animal
296 systems to plants and refining these methods for stable, low-cost generation of sequencing libraries
297 from small amounts of RNA starting material. This allows the design of experiments in which spatial
298 information is required but only small pieces of tissue can be obtained. In the process of method
299 development, we tested and included several features to efficiently generate double stranded cDNA
300 (ds-cDNA) with reduced PCR amplification in both ds-cDNA synthesis and subsequent amplification
301 after Nextera tagmentation. We introduced sample specific barcodes in the Nextera amplification
302 step to allow pooling of 2304 of samples per sequencing run. This optimisation altogether allowed us
303 to construct sequencing libraries by hand for just £ 6.00 per library (see **Additional_file2.xlsx**) in
304 comparison to £ 65.56 for an Illumina TruSeq library (RS-122-2001, Illumina) or £ 62.60 for a
305 SMARTer PCR cDNA Synthesis Kit library (634926, TaKaRa).

306 In our benchmarking experiments we compared the Grid-seq workflow with the widely used Illumina
307 TruSeq sequencing protocol and show that the Grid-seq method compares well with this common
308 commercial RNA-seq protocol (see: **Additional_file1.docx**). We also show that Grid-seq can detect

309 transcript level differences across 1D leaf sections in distinct leaf elements such as leaf margins or
310 vascular tissues and that spatial mapping of transcript levels to specific sections of leaves is possible,
311 which allows drawing of transcriptional expression profiles across tissues. This easily used, low cost
312 protocol makes feasible experiments that require spatial transcriptome analysis.

313 To apply the Grid-seq method for studying biotic actions we challenged *A. thaliana* leaves with the
314 bacterial peptide flg22, a conserved 22 amino acid sequence of the bacteria flagellin protein, which
315 to the plant indicates an encounter with potentially pathogenic bacteria [35]. Plants recognize such
316 potential threats as the pathogenic cell surface molecules, so called Pathogen-Associated Molecular
317 Patterns (PAMPs), perceived by the plant Pattern Recognition Receptors (PRRs) on the plant cell
318 surface [36]. This event initiates an intracellular plant signalling cascade leading eventually to
319 immunity or disease [17,37]. In our experiments we could detect the triggering of immune and
320 defence response related biological processes and show that the results obtained by RNA-seq are
321 independently reproducible using qRT-PCR (see: **Additional_file1.docx**). We were able to find
322 overlap in our data with already described flg22 elicited (FLARE) genes from a gross-scale experiment
323 using a strong stimulus [18]. In comparative analyses of our dataset with the spatial expression
324 patterns of the described FLARE genes we were able to identify genes which share similar spatial
325 expression and are potential novel FLARE genes. Cluster based analysis of spatial expression data
326 revealed sets of genes with highly similar expression profiles enriched in distinct biological processes;
327 including FLARE genes to which we add new and increased expression resolution. Characterisation of
328 spatial cluster expression profiles highlighted plant regulatory elements with local or spatially
329 elevated expression levels and so potential short distance signal propagators upon flg22 stimulus.

330 In a proof of principle experiment applying of the oomycte *Albugo laibachii NC14* to *A. thaliana*
331 leaves we also recovered both host and pathogen transcript data, indicating that dual-host pathogen
332 experiments (between eukaryotic organisms) are possible (see: **Additional_file1.docx** and
333 **Additional_file2.xlsx**).

334 **Conclusions**

335 We find that Grid-seq allows reproducible spatial-transcriptome experiments in plant tissues. Proof
336 of concept experiments highlighted the usability of the method in characterising spatial differences
337 within organs, and changes induced by biotic stimuli of bacterial PAMPs. The workflow also
338 compares well to widely used RNA-seq protocols such as Illumina TruSeq sequencing but can be
339 conducted at a fraction (~ 1/10th) of the library preparation costs of Illumina TruSeq. Furthermore,
340 as our ds-cDNA synthesis method is based on single-cell technologies [33], even smaller sections
341 could be processed while maintaining efficient library and sequencing results.

342 **Methods**

343 **Plant growth**

344 For our experiments we used 4 – 6 week old *A. thaliana* Col-0 plants that were grown in a controlled
345 environment room with an 8 hours light, 16 hour dark cycle at a constant temperature of 22 °C and
346 70 % humidity.

347 **Flg22 exposure experiments**

348 Before flg22 treatment experiments, we transferred the plants from the controlled environment
349 room to a laboratory working bench (room with constant light exposure and temperature). To elicit
350 plant responses with flg22 we either syringe infiltrated [38] the peptide or spotted a droplet of flg22
351 on a leaf using a pipette.

352 To produce small, local infiltration spots we used a 1 ml syringe (BS01T, R&L Slaughter Ltd, Basildon,
353 UK) loaded with 500 nM flg22 peptide solution. By application of mild pressure on the plunger of the
354 syringe when infiltrating we produced an approximately 2 - 3 mm diameter infiltration spot on the
355 left-hand side of a leaf. In parallel to flg22 infiltration we produced an infiltration series with
356 DNase/RNase-free water as control. The plants were subsequently incubated on the laboratory
357 working bench for 1 hour until sampling.

358 For the flg22 spotting experiment we loaded a 1 µl droplet of 500 nM flg22 on the abaxial surface of
359 a leaf using a pipette (diameter approximately 1 mm). The flg22 was pipetted onto the left half of the
360 leaf and a 1 µl droplet of the water control droplet spotted on the right half of the leaf. After spotting
361 the plants were incubated for 1 hour on the laboratory bench before sampling.

362 **Leaf sectioning and sample harvesting**

363 We used single margin razor blades (T586, Agar Scientific Ltd., Stansted, UK) to cut leaves into
364 approximately 1 mm^2 small leaf squares. To create a clean surface for cutting we used the pealed,
365 non-sticky paper cover of a 96-well plate seal (AB0580, Thermo Fisher Scientific, Waltham, USA).
366 With a previously in RNaseZAP (AM9780, Thermo Fisher Scientific, Waltham, USA) washed and air-
367 dried forceps (T083, TAAB Laboratories Equipment Ltd, Berks, UK) we transferred each leaf square
368 immediately after cutting into a well of a 96-well plate (E1403-0100-C, Starlab, Milton Keynes, UK)
369 which we had pre-cooled on a 96-well metal block in dry ice (- 70 ^{o}C), or alternatively, a dry-ice
370 cooled 1.5 ml tube (10051232, Fisher Scientific, Loughborough, UK). The sample wells of 96-well
371 plates were sealed using domed PCR cap strips (AB0602, Thermo Fisher Scientific, Waltham, USA).
372 Post harvesting the samples were stored at -80 ^{o}C until use.

373 **Leaf sample lysis and preparation for mRNA extraction**

374 To lyse the leaf samples stored in 1.5 ml tubes we first added 10 µl lysis buffer composed of 100 mM
375 Tris-HCl pH 7.5 (BP1757, Fisher Scientific, Loughborough, UK), 500 mM LiCl (L7026, Sigma Aldrich, St.
376 Louis, USA), 10 mM EDTA pH 8.0 (E7889, Sigma Aldrich, St. Louis, USA), 1% LiDS (L4632, Sigma
377 Aldrich, St. Louis, USA), 5 mM DTT (18064014, Thermo Fisher Scientific, Waltham, USA) to each
378 sample immediately after removing the sample tube from the cold storage.

379 We subsequently ground the leaf sections in lysis buffer using polypropylene pestles (Z359947, Sigma
380 Aldrich, St. Louis, USA), which, before use, were washed with RNaseZAP (R2020, Sigma Aldrich, St.
381 Louis, USA, three times with 80% ethanol (32221, Sigma Aldrich, St. Louis, USA) rinsed with UltraPure
382 DNase/RNase-Free Distilled Water (10977049, Thermo Fisher Scientific, Waltham, USA) and air-dried

383 after washing. After sample lysis we transferred the lysate to an ice-cooled 96-well plate and
384 continued with the mRNA extraction.

385 Samples stored in 96-well plates were lysed by using 1 mm diameter grade 1000 hardened 1010
386 carbon steel ball bearings (Simply Bearings Ltd, Leigh, UK). For this, before use of the ball bearings,
387 we treated a bulk batch sequentially with RNaseZAP and DNA AWAY, after this washed the ball
388 bearings three times with 80% ethanol and transferred them to sterile screw-cap 2.0 ml tubes
389 (E1420-2341, Starlab, Milton Keynes, UK) and heat dried with a slightly loosened lid on a 95 ^{o}C
390 heating block (N2400-4001, Starlab, Milton Keynes, UK).

391 To lyse the collected leaf samples stored in a 96-well plate, we transferred the 96-well plate to a dry
392 ice temperature cooled 96-well metal block. We carefully opened the domed PCR cap lids to avoid
393 sample spillage and added the 4 – 6 (room temperature) ball bearings to each sample well. After this
394 we transferred 10 µl lysis buffer to each well and re-sealed the plate with new domed PCR cap lids,
395 and immediately proceeded to the 2010 Geno/Grinder (SPEX SamplePrep, Stanmore, UK) disrupting
396 the samples for 30 seconds at 1750 rpm. We gathered the sampled using a centrifuge (Centrifuge
397 5910 R, Eppendorf UK Ltd, Stevenage, UK) for 10 seconds at 2000 x rcf. A strongly green-coloured
398 solution without any remaining solid leaf material indicated good sample lysis. If satisfactory sample
399 lysis was not achieved, we disrupted the samples again for another 10 seconds on the 2010
400 Geno/Grinder at 1750 rpm and centrifuged for 30 seconds at 2000 x rcf. We immediately transferred
401 the lysis solutions into a new 96-well plate using a 10 µl multichannel pipette. After transfer of the
402 lysis solutions, we stored the new 96-well plate on ice, discarded the 96-well plate containing the ball
403 bearings and proceeded immediately with mRNA extraction. For a laboratory compatible version of
404 the workflow see: **Additional_file1.docx**.

405 **Leaf mRNA purification**

406 The leaf tissue mRNA was purified using 1 µl NEBNext Poly(A) mRNA Magnetic Isolation Module
407 oligo-dT(25) beads (E7490, New England Biolabs Ltd, Hitchin, UK) per extraction. Previous to the

408 extraction the required volume of oligo-dT(25) magnetic beads was washed twice in 200 µl lysis
409 buffer on a DynaMag-2 Magnet rack (12321D, Thermo Fisher Scientific, Waltham, USA) and
410 resuspended in 10 µl lysis buffer for each 1 µl oligo-dT(25) beads input volume. The beads were
411 mixed by a quick vortex and 10 µl of the resuspended beads were transferred to each well of the 96-
412 well plate containing the lysis solutions. The wells were sealed with domed PCR cap strips, the 96-
413 well plate vortexed briefly and attached to a tube rotator (444-0502, VWR International Ltd,
414 Luterworth, UK) with adhesive tape. After 10 minutes rotation we collected the lysis solution at the
415 bottom of the wells by spinning the plate for 10 seconds at 2000 x rcf and pelleted the oligo-dT(25)
416 magnetic beads on a 96-ring magnetic plate (A001219, Alpaqua, Beverly, USA). Using a multichannel
417 pipette we washed the oligo-dT(25) magnetic beads twice with 50 µl Wash Buffer A (10mM Tris-HCl
418 pH7.5, 0.15M LiCl, 1mM EDTA, 0.1% LiDS) and once with Wash Buffer B (10mM Tris-HCl pH 7.5,
419 0.15M LiCl, 1mM EDTA). After washing we centrifuged the plate for 10 seconds at 2000 x rcf to
420 collect the remaining Wash Buffer B at the bottom of the tube, pelleted the oligo-dT(25) magnetic
421 beads on a magnet and removed the remaining volume of Wash Buffer B with a multichannel
422 pipette. The oligo-dT(25) beads were resuspended immediately in 8 µl DNase/RNase-Free water,
423 incubated for 2 minutes at 80 ^{o}C on a G-Storm GS1 thermal cycler (G-Storm, Somerton, UK), then
424 immediately pelleted on a 96-ring magnetic plate to elute the mRNA off and separate from the oligo-
425 dT(25) beads. The solutions containing the purified mRNA were immediately transferred to a new 96-
426 well plate, which was placed in a - 80 ^{o}C freezer until needed. For a laboratory compatible version of
427 the workflow see: **Additional_file1.docx**.

428 **Double-stranded cDNA synthesis reaction**

429 For ds-cDNA synthesis we used a protocol based on the template switching mechanism of the
430 reverse transcriptase enzymes [39]. Briefly: 2.50 µl extracted mRNA was mixed with 2 µl 5x First
431 Strand buffer (18064014, Thermo Fisher Scientific, Waltham, USA), 1 µl 10 mM dNTPs (10297018,
432 Thermo Fisher Scientific, Waltham, USA), 1 µl 5'-biotinylated 10 µM STRT-V3-T30-VN oligonucleotide:
433 5'-/5Biosg/TTAAGCAGTGGTATCAACGCAGAGTCGACTTTTTTTTTTTTTTTTTTTTTTTTTTTTTVN-3'

434 (Integrated DNA Technologies, Leuven, BE), 1 µl 20 mM DTT (18064014, Thermo Fisher Scientific,
435 Waltham, USA), 0.10 µl 40 U/µl RNase Inhibitor (M0314S, New England Biolabs Ltd, Hitchin, UK), 0.25
436 µl 10 µM template switching oligo 5'-
437 AAGCAGTGGTATCAACGCAGAGTGCAGUGCUTGATGATGGrGrGrG-3' (Integrated DNA Technologies,
438 Leuven, BE), 0.30 µl 200 U/µl SuperScript II Reverse Transcriptase (18064014, Thermo Fisher
439 Scientific, Waltham, USA), 0.30 µl 100 µM $MnCl_2$ (M1787, Sigma Aldrich, St. Louis, USA) and 1.55 µl
440 DNase/RNase-Free water to a total reaction volume of 10 µl. The reverse transcription reaction was
441 run in a G-Storm GS1 thermal cycler for 90 minutes at 42 ^{o}C with additional 10 minutes at 72 ^{o}C to
442 inactivate the reverse transcriptase. After reverse transcription we immediately added 2 µl RNase H
443 (M0297S, New England Biolabs Ltd, Hitchin, UK) diluted to 0.5 U/µl (5 U/µl stock concentration) to
444 the reaction and incubated the reaction in the GS1 thermal cycler for 30 minutes at 37 ^{o}C. The RNase
445 H treated reactions were purified using a 0.83x (10 µl) AMPure XP bead ratio (Beckman Coulter, High
446 Wycombe, UK) and eluted in 18 µl 1x TE buffer. After this step we added 5 µl 5x Kapa HiFi PCR buffer
447 (KK2102, KAPA BioSystems, Wilmington, USA), 0.75 µl 10 mM dNTPs, 0.75 µl 10 µM PCR+G primer 5'-
448 GAAGCAGTGGTATCAACGCAGAGT-3' (Integrated DNA Technologies, Leuven, BE) and 0.50 µl 1 U/µl
449 Kapa HiFi polymerase (KK2102, KAPA BioSystems, Wilmington, USA) to the cleaned ds-cDNA resulting
450 in a total reaction volume of 25 µl and amplified the ds-cDNA in a G-Storm GS1 thermal cycler
451 according to the following programme: (1) 3 minutes at 94 ^{o}C, (2) 17 cycles with 30 seconds at 94 ^{o}C,
452 30 seconds at 63 ^{o}C and 1 minute 30 seconds at 72 ^{o}C, (3) a final elongation step for 5 minutes at 72
453 ^{o}C. The amplified libraries were purified using a 1x (25 µl) AMPure XP bead ratio and eluted in 20 µl
454 1x TE buffer. The ds-cDNA libraries could be stored at this point in a -20 ^{o}C freezer. Before continuing
455 with Illumina sequencing library preparation, we measured the ds-cDNA library concentrations with
456 the Qubit 2.0 Fluorometer (Thermo Fisher Scientific, Waltham, USA) dsDNA HS Assay Kit reagents
457 (Q32854, Thermo Fisher Scientific, Waltham, USA) and also assessed the size distributions of
458 randomly picked libraries on an Agilent Bioanalyser (G2939BA, Agilent Technologies, Stockport, UK)
459 using the Agilent High Sensitivity DNA Kit (5067-4626, Agilent Technologies, Stockport, UK).

460 At later stages we modified the ds-cDNA synthesis integrating elements of the Smart-seq2 protocol
461 [40]. The reverse transcription reactions of Grid-seq-1.0 (as described above) and Smart-seq2 were
462 already highly similar, but Smart-seq2 had proven to require less hands-on time than the Grid-seq-
463 1.0 reverse transcription workflow. Grid-seq-1.1 uses the Smart-seq2 ds-cDNA synthesis with minor
464 modifications, briefly: 2.50 µl extracted mRNA were combined with 1 µl 10 µM Smart-seq2 Oligo-
465 dT30VN (5'-AAGCAGTGGTATCAACGCAGAGTACTTTTTTTTTTTTTTTTTTTTTTTTTTTTTTVN-3', Integrated
466 DNA Technologies, Leuven, BE) and 1 µl 10 mM dNTPS to a total volume of 4.5 µl. To anneal the
467 Smart-seq2 Oligo-dT30VN we incubated the library for 30 seconds at 72 ^{o}C and snap-cooled the
468 mixture on ice. The reverse transcription was conducted by adding the following reagents to the
469 reaction with a final reaction volume of 10 µl: 2 µl 5x First Strand buffer, 2 µl 5 M betaine (B0300,
470 Sigma Aldrich, St. Louis, USA), 1 µl 1 M $MgCl_2$ (AM9530G, Thermo Fisher Scientific, Waltham, USA),
471 0.5 µl 100 mM DTT, 0.25 µl 40 U/µl RNase Inhibitor (2313A, Takara Clontech, Mountain View, USA),
472 0.10 µl 10 µM Smart-seq2 template switching oligo (5'-AAGCAGTGGTATCAACGCAGAGTACATrGrG+G-
473 3', Exiqon, Vedbaek, DK), 0.50 µl 200 U/µl SuperScript II Reverse Transcriptase, and 0.09 µl
474 DNase/RNase-free water. We performed the reverse transcription reaction for (1) 90 minutes at 42
475 ^{o}C, (2) 15 cycles with 2 minutes at 50 ^{o}C and 2 minutes at 42 ^{o}C and finally (3) 15 minutes at 70 ^{o}C.
476 After reverse transcription we added 12.50 µl 2x Kapa HiFi HotStart ReadyMix (KK2601, KAPA
477 BioSystems, Wilmington, USA), 0.25 µl 10 µM Smart-seq2 IS-PCR primers (Integrated DNA
478 Technologies, Leuven, BE) and 2.25 µl DNase/RNase-Free water to the reaction resulting in a total
479 volume of 15 µl per reaction. Amplification was performed in a G-Storm GS1 cycler according to the
480 programme: (1) 3 minutes at 98 ^{o}C, (2) 15 cycles with 20 seconds at 98 ^{o}C, 15 seconds at 67 ^{o}C and 6
481 minutes at 72 ^{o}C and a (3) final elongation step for 5 minutes at 72 ^{o}C. The PCR reactions were
482 purified using a 0.65 x (9.75 µl) AMPure XP cleanup and eluted in 20 µl 1 x TE buffer. After cleanup
483 we measured the ds-cDNA library concentrations with the Qubit 2.0 Fluorometer dsDNA HS Assay Kit
484 reagents and loaded randomly selected libraries on the Agilent Bioanalyser using the Agilent High

485 Sensitivity DNA Kit before continuing with Illumina sequencing library prepration. For a laboratory
486 compatible version of the workflow see: **Additional_file1.docx**.

487 **Illumina library preparation from ds-cDNA**

488 We prepared Illumina sequencing libraries using an Illumina Nextera (FC-121-1030, Illumina
489 Cambridge, UK) based protocol with minor modifications: we exclusively used the Tagment DNA
490 Enzyme 1 and the Tagment DNA Buffer and amplified the tagmented DNA with the Kapa 2G Robust
491 Polymerase (KK5024, Sigma Aldrich, St. Louis, USA). We used custom Nextera barcodes that allow us
492 to multiplex hundreds of samples (see: **Additional_file2.xlsx**) [41].

493 We reduced the costs of the library preparation by reducing the total tagmentation reaction volume
494 to 5 µl (from 50 µl as recommended) with 1 ng ds-cDNA library input and using less enzyme. We
495 performed a titration experiment of Tagment DNA Enyzme vs. 1 ng of selected ds-cDNA libraries
496 aiming for Illumina sequencing libraries with a modal insert size distribution in the range of 400-500
497 bp with little short insert fragments and found that 0.1 µl Nextera enzyme was optimal.

498 The Nextera reactions were performed by combining 1 ng of ds-cDNA (air-dried over-night at room
499 temperature in a drawer with the 96-well plate loosely covered to allow evaporation of liquid) with
500 2.5 µl 2 x Nextera buffer, 2.4 µl water and 0.1 µl Nextera enzyme on ice. The tagmentation plate was
501 immediately transferred for 5 minutes at 55 ^{o}C on a G-Storm GS1 thermal cycler. Meanwhile we
502 prepared a fresh 96-well plate with 2.0 µl 2.5 µM P5 and 2.0 µl 2.5 µM P7 custom multiplexing
503 primers (see: **Additional_file2.xlsx**). After tagmentation we transferred the tagmentation reactions
504 to the previously prepared 96-well plate containing the sequencing adapters (see above) and added
505 the following to each well: 5.00 µl 5 x Kapa 2G Robust Buffer, 0.50 µl 10 mM dNTPs, 0.10 µl 5 U / µl
506 Kapa 2G Robust Polymerase, 10.4 µl water to a total final volume of 25 µl.

507 Amplification was performed on a GStorm GS-1 cycler using the following program: (1) 3 minutes at
508 72 ^{o}C, 1 minute at 95 ^{o}C (2) 11 cycles of 10 seconds at 95 ^{o}C, 30 seconds at 65 ^{o}C, 2 minutes 30
509 seconds at 72 ^{o}C (2) a final elongation step for 2 minutes 30 seconds at 72°C. After amplification we

510 purified the libraries using a 0.64x ratio (16 µl) AMPure XP beads, measured the library yields with
511 the Qubit 2.0 Fluorometer dsDNA HS Assay Kit reagents and assessed the size distributions of
512 randomly selected libraries on the Agilent Bioanalyser with the Agilent High Sensitivity DNA Kit. For a
513 laboratory compatible version of the workflow see: **Additional_file1.docx**.

514 **Sample pooling and sequencing**

515 For sequencing all library concentrations were determined using Qubit 2.0 Fluorometer using the
516 dsDHA HS Assay kit reagents and pooled at equal molarity. The profile and concentration of the final
517 library pool was assessed on the Agilent Bioanalyser using Agilent High Sensitivity DNA Kit
518 Sequencing reagents. After this the pooled samples were shipped to the Earlham Institute for
519 sequencing. Quality control and data demultiplexing was performed by the Earlham Institute
520 Genomics Pipelines facilities. Samples were sequenced using Illumina HiSeq2500 50 base single-end
521 rapid run sequencing for the *A. thaliana* wounding and *A. thaliana* flg22 infiltration datasets Illumina
522 NextSeq500 75 base single-end for the *A. thaliana* untreated leaf dataset and Illumina HiSeq4000 150
523 base paired-end sequencing for the *A. thaliana* flg22 droplet spotting experiment.

524 **Data quality control and mapping**

525 The sequencing reads were quality controlled using FastQC-0.11.5 [42]. After quality control we used
526 cutadapt-1.17 [43] to trim low-quality bases (-q 20) and remove Oligo-dT, template switching oligos,
527 primer and Illumina Nextera library preparation sequences (-n 5 -e 0.05 –overlap 10). We also
528 removed sequences with less than 40 bases (--minimum-length 40) and sequences containing N's (--
529 max-n 0) from the dataset with cutadapt-1.17. After adapter and quality trimming we re-assessed
530 the reads a second time with FastQC-0.11.5. We mapped the reads to the *A. thaliana* TAIR10 release
531 37 genome assembly using STAR-2.5.1b [44] default settings and assessed mapping scores,
532 duplication levels, GC-bias and gene-body coverage after mapping with RSeQC-2.6.4 [45]. Reads were
533 counted with HTSeq-count-0.6.0 [46] default settings.

534 **Differential-expression analysis, GO-term enrichment and plant metabolic pathway enrichment**

535 Differential expression analysis was performed using DESEq2-1.20.0 [47] in the statistical language R-
536 3.5.1 using the workflow described by Love et al. [48] but by pre-filtering the dataset for rows with
537 less than 10 rather than 1 raw read counts. DE-genes were called with a q-value threshold < 0.05%.

538 Across leaf DE-gene expression plots were prepared using R-3.5.1; in brief: We imported all samples
539 with DESeq2-1.20.0 and calculated a table with normalised expression values as in the workflow
540 described by Love et al. [48]. Next, we calculated the average expression value of each gene in each
541 leaf square across all biological replicates. As a final step we normalised the expression values of the
542 leaf squares. For this we divided the mean expression value of each leaf square of a gene with the
543 mean expression value across all leaf squares of the same gene. The log2 transformed plots of the so
544 normalised data were generated using ggplot2-3.1.0 [49]. Affinity propagation clustering of the
545 normalised expression tables was performed using the R-3.5.1 library apcluster-1.4.7 and a Pearson
546 distance matrix of the normalised data for apclustK and apclust [21] default settings. The number of
547 clusters was either empirically determined by continuously increasing the preferred cluster number
548 in the apclustK function and visualising the expression profiles of the clusters using ggplot2-3.1.0 or
549 determined without providing a cluster number preference value using the apclust function.

550 GO-term enrichment analysis on DE-genes was performed using the R-3.5.1 Bioconductor library
551 ClusterProfiler-3.8.1 [50] with the settings (Statistical test: Hypergeometric test, Multiple testing
552 correction: Benjamini & Hochberg False Discovery Rate correction, False Discovery Rate cutoff: 0.01)
553 and the Bioconductor library org.At.tair.db-3.6.0 as organism database [51].

554 **Additional files**

555 **Additional_file1.docx:** Comparison of Grid-seq with Illumina TruSeq, qRT-PCR validation of DE gene
556 expression, wounding time-series GO enrichment, *Albugo laibachii* spatial transcriptomics
557 experiment, all wet-lab protocols of the Grid-seq workflow.

558 **Additional_file2.xlsx:** Read numbers, ENA accessions, DE genes, GO accessions, clustering
559 information, FLARE associations of experiments.

560 **Additional_file3.xlsx:** GO-term enrichments of spatial affinity propagation clustering.

561 **Ethics approval and consent to participate**

562 Not applicable.

563 **Consent for publication**

564 This study abides by UK guidelines and legislation for plant science research.

565

566 **Availability of data and material**

567 Sequencing reads for the Grid-seq vs. TruSeq comparison are available under the ENA study
568 accession number PRJEB31337. Sequencing reads for the wounding experiment are available under
569 the ENA study accession number PRJEB31311. Sequencing reads for the untreated leaf spatial
570 transcriptomics experiment are available under the ENA study accession number PRJEB31314.
571 Sequencing reads for the flg22 / water infiltration experiment are available under the ENA study
572 accession number PRJEB31312. Sequencing reads for the flg22 / water droplet spotting experiment
573 are available under the ENA study accession number PRJEB31313. Sequencing reads for the *Albugo*
574 *laibachii* x *Arabidopsis.thaliana* spatial transcriptomics experiment are available under the ENA study
575 accession number PRJEB31803.

576 **Competing Interests**

577 The authors declare no competing interests.

578 **Funding**

579 This work was strategically funded by the Biotechnology and Biological Sciences Research Council
580 (BBSRC), Institute Strategic Programme Grant (BB/J004669/1) at the Earlham Institute (formerly The
581 Genome Analysis Centre, Norwich), a BBSRC National Capability Grant (BB/J010375/1), a BBSRC Core

582 Strategic Programme Grant (BB/CSP17270/1), a BBSRC DTP Studentship Award (BB/M011216/1) and
583 by the Natural History Museum.

584 **Authors' contributions**

585 M.G., W.V. and D.H. established protocols. M.G., W.V. and A.L. prepared sequencing libraries. M.G.
586 analysed the data. I.M. advised on protocols and data analysis. M.G. and M.D.C. wrote the
587 manuscript. W.V., M.G. and M.D.C. designed the study.

588 **Acknowledgements**

589 We thank David Prince for providing the *A. laibachii* NC14.

590 **References**

591 1. Müller B, Grossniklaus U. Model organisms — A historical perspective. J Proteomics.
592 2010;73:2054–63.

593 2. Mincarelli L, Lister A, Lipscombe J, Macaulay IC. Defining Cell Identity with Single-Cell Omics.
594 PROTEOMICS. 2018;1700312.

595 3. Crosetto N, Bienko M, van Oudenaarden A. Spatially resolved transcriptomics and beyond. Nat Rev
596 Genet. 2015;16:57–66.

597 4. Stahl PL, Salmen F, Vickovic S, Lundmark A, Navarro JF, Magnusson J, et al. Visualization and
598 analysis of gene expression in tissue sections by spatial transcriptomics. Science. 2016;353:78–82.

599 5. Junker JP, Noël ES, Guryev V, Peterson KA, Shah G, Huisken J, et al. Genome-wide RNA
600 Tomography in the Zebrafish Embryo. Cell. 2014;159:662–75.

601 6. Giacomello S, Salmén F, Terebieniec BK, Vickovic S, Navarro JF, Alexeyenko A, et al. Spatially
602 resolved transcriptome profiling in model plant species. Nat Plants. 2017;3:17061.

603 7. Rusk N. Genomics: Spatial transcriptomics. Nat Methods. 2016;13:710–1.

604 8. Mulema JMK, Denby KJ. Spatial and temporal transcriptomic analysis of the Arabidopsis thaliana-
605 Botrytis cinerea interaction. Mol Biol Rep. 2012;39:4039–49.

606 9. Ghawana S, Paul A, Kumar H, Kumar A, Singh H, Bhardwaj PK, et al. An RNA isolation system for
607 plant tissues rich in secondary metabolites. BMC Res Notes. 2011;4:85.

608 10. Borges F, Gardner R, Lopes T, Calarco JP, Boavida LC, Slotkin R, et al. FACS-based purification of
609 Arabidopsis microspores, sperm cells and vegetative nuclei. Plant Methods. 2012;8:44.

610 11. Deal RB, Henikoff S. The INTACT method for cell type–specific gene expression and chromatin
611 profiling in Arabidopsis thaliana. Nat Protoc. 2010;6:56.

612 12. Gaiero P, Šimková H, Vrána J, Santiñaque FF, López-Carro B, Folle GA, et al. Intact DNA purified
613 from flow-sorted nuclei unlocks the potential of next-generation genome mapping and assembly in
614 Solanum species. MethodsX. 2018;5:328–36.

615 13. Duncan S, Olsson T, Hartley M, Dean C, Rosa S. Single Molecule RNA FISH in Arabidopsis Root
616 Cells. BIO-Protoc [Internet]. 2017 [cited 2018 Jul 5];7. Available from: https://bio-protocol.org/e2240

617 14. Kerk NM. Laser Capture Microdissection of Cells from Plant Tissues. PLANT Physiol. 2003;132:27–
618 35.

619 15. Chan AC, Khan D, Girard IJ, Becker MG, Millar JL, Sytnik D, et al. Tissue-specific laser
620 microdissection of the *Brassica napus* funiculus improves gene discovery and spatial identification of
621 biological processes. J Exp Bot. 2016;67:3561–71.

622 16. Martin LBB, Nicolas P, Matas AJ, Shinozaki Y, Catalá C, Rose JKC. Laser microdissection of tomato
623 fruit cell and tissue types for transcriptome profiling. Nat Protoc. 2016;11:2376–88.

624 17. Jones JDG, Dangl JL. The plant immune system. Nature. 2006;444:323–9.

625 18. Navarro L. The Transcriptional Innate Immune Response to flg22. Interplay and Overlap with Avr
626 Gene-Dependent Defense Responses and Bacterial Pathogenesis. PLANT Physiol. 2004;135:1113–28.

627 19. Farmer E, Farmer E, Mousavi S, Lenglet A. Leaf numbering for experiments on long distance
628 signalling in Arabidopsis. Protoc Exch [Internet]. 2013 [cited 2016 Nov 3]; Available from:
629 http://www.nature.com/protocolexchange/protocols/2787

630 20. Supek F, Bošnjak M, Škunca N, Šmuc T. REVIGO Summarizes and Visualizes Long Lists of Gene
631 Ontology Terms. Gibas C, editor. PLoS ONE. 2011;6:e21800.

632 21. Frey BJ, Dueck D. Clustering by Passing Messages Between Data Points. Science. 2007;315:972–6.

633 22. Berardini TZ, Reiser L, Li D, Mezheritsky Y, Muller R, Strait E, et al. The arabidopsis information
634 resource: Making and mining the "gold standard" annotated reference plant genome: Tair: Making
635 and Mining the "Gold Standard" Plant Genome. genesis. 2015;53:474–85.

636 23. Pandey SP, Somssich IE. The Role of WRKY Transcription Factors in Plant Immunity. PLANT
637 Physiol. 2009;150:1648–55.

638 24. Xie Z, Nolan TM, Jiang H, Yin Y. AP2/ERF Transcription Factor Regulatory Networks in Hormone
639 and Abiotic Stress Responses in Arabidopsis. Front Plant Sci. 2019;10:228.

640 25. Dubos C, Stracke R, Grotewold E, Weisshaar B, Martin C, Lepiniec L. MYB transcription factors in
641 Arabidopsis. Trends Plant Sci. 2010;15:573–81.

642 26. Kulkarni SR, Vaneechoutte D, Van de Velde J, Vandepoele K. TF2Network: predicting transcription
643 factor regulators and gene regulatory networks in Arabidopsis using publicly available binding site
644 information. Nucleic Acids Res. 2018;46:e31–e31.

645 27. Iwata Y, Fedoroff NV, Koizumi N. *Arabidopsis* bZIP60 Is a Proteolysis-Activated Transcription
646 Factor Involved in the Endoplasmic Reticulum Stress Response. Plant Cell. 2008;20:3107–21.

647 28. Ryu KH, Huang L, Kang HM, Schiefelbein J. Single-Cell RNA Sequencing Resolves Molecular
648 Relationships Among Individual Plant Cells. Plant Physiol. 2019;179:1444–56.

649 29. Denyer T, Ma X, Klesen S, Scacchi E, Nieselt K, Timmermans MCP. Spatiotemporal Developmental
650 Trajectories in the Arabidopsis Root Revealed Using High-Throughput Single-Cell RNA Sequencing.
651 Dev Cell. 2019;48:840-852.e5.

652 30. Jean-Baptiste K, McFaline-Figueroa JL, Alexandre CM, Dorrity MW, Saunders L, Bubb KL, et al.
653 Dynamics of gene expression in single root cells of A. thaliana. Plant Cell. 2019;tpc.00785.2018.

654 31. Karasov TL, Almario J, Friedemann C, Ding W, Giolai M, Heavens D, et al. Arabidopsis thaliana and
655 Pseudomonas Pathogens Exhibit Stable Associations over Evolutionary Timescales. Cell Host Microbe.
656 2018;24:168-179.e4.

657 32. Dangl JL, Horvath DM, Staskawicz BJ. Pivoting the Plant Immune System from Dissection to
658 Deployment. Science. 2013;341:746–51.

659 33. Picelli S, Faridani OR, Björklund ÅK, Winberg G, Sagasser S, Sandberg R. Full-length RNA-seq from
660 single cells using Smart-seq2. Nat Protoc. 2014;9:171–81.

661 34. Macaulay IC, Haerty W, Kumar P, Li YI, Hu TX, Teng MJ, et al. G&T-seq: parallel sequencing of
662 single-cell genomes and transcriptomes. Nat Methods. 2015;12:519–22.

663 35. Denoux C, Galletti R, Mammarella N, Gopalan S, Werck D, De Lorenzo G, et al. Activation of
664 Defense Response Pathways by OGs and Flg22 Elicitors in Arabidopsis Seedlings. Mol Plant.
665 2008;1:423–45.

666 36. Zipfel C. Pattern-recognition receptors in plant innate immunity. Curr Opin Immunol. 2008;20:10–
667 6.

668 37. Bent A. Resistance from relatives. Nat Biotechnol. 2016;34:620–621.

669 38. Underwood W, Somerville SC. Perception of conserved pathogen elicitors at the plasma
670 membrane leads to relocalization of the Arabidopsis PEN3 transporter. Proc Natl Acad Sci.
671 2013;110:12492–7.

672 39. Zhu YY, Machleder EM, Chenchik A, Li R, Siebert PD. Reverse transcriptase template switching: a
673 SMART approach for full-length cDNA library construction. BioTechniques. 2001;30:892–7.

674 40. Picelli S, Björklund \AAsa K., Faridani OR, Sagasser S, Winberg G, Sandberg R. Smart-seq2 for
675 sensitive full-length transcriptome profiling in single cells. Nat Methods [Internet]. 2013 [cited 2015
676 Jan 6]; Available from: http://www.nature.com/nmeth/journal/vaop/ncurrent/full/nmeth.2639.html

677 41. Beier S, Himmelbach A, Colmsee C, Zhang X-Q, Barrero RA, Zhang Q, et al. Construction of a map-
678 based reference genome sequence for barley, Hordeum vulgare L. Sci Data. 2017;4:170044.

679 42. FastQC: a quality control tool for high throughput sequence data. 2010.
680 http://www.bioinformatics.babraham.ac.uk/projects/fastqc. Accessed 31 Jan 2017.

681 43. Martin M. Cutadapt removes adapter sequences from high-throughput sequencing reads.
682 EMBnet J. 2011;17:pp–10.

683 44. Dobin A, Gingeras TR. Mapping RNA-seq Reads with STAR: Mapping RNA-seq Reads with STAR. In:
684 Bateman A, Pearson WR, Stein LD, Stormo GD, Yates JR, editors. Curr Protoc Bioinforma [Internet].
685 Hoboken, NJ, USA: John Wiley & Sons, Inc.; 2015 [cited 2017 Jan 9]. p. 11.14.1-11.14.19. Available
686 from: http://doi.wiley.com/10.1002/0471250953.bi1114s51

687 45. Wang L, Wang S, Li W. RSeQC: quality control of RNA-seq experiments. Bioinforma Oxf Engl.
688 2012;28:2184–5.

689 46. Anders S, Pyl PT, Huber W. HTSeq--a Python framework to work with high-throughput sequencing
690 data. Bioinformatics. 2015;31:166–9.

691 47. Love MI, Huber W, Anders S. Moderated estimation of fold change and dispersion for RNA-seq
692 data with DESeq2. Genome Biol [Internet]. 2014 [cited 2017 May 31];15. Available from:
693 http://genomebiology.biomedcentral.com/articles/10.1186/s13059-014-0550-8

694 48. Love MI, Anders S, Kim V, Huber W. RNA-Seq workflow: gene-level exploratory analysis and
695 differential expression. F1000Research. 2016;4:1070.

696 49. Wickham H. Ggplot2: elegant graphics for data analysis. New York: Springer; 2009.

697 50. Yu G, Wang L-G, Han Y, He Q-Y. clusterProfiler: an R Package for Comparing Biological Themes
698 Among Gene Clusters. OMICS J Integr Biol. 2012;16:284–7.

699 51. Carlson M. org.At.tair.db: Genome wide annotation for Arabidopsis. 2018.

700

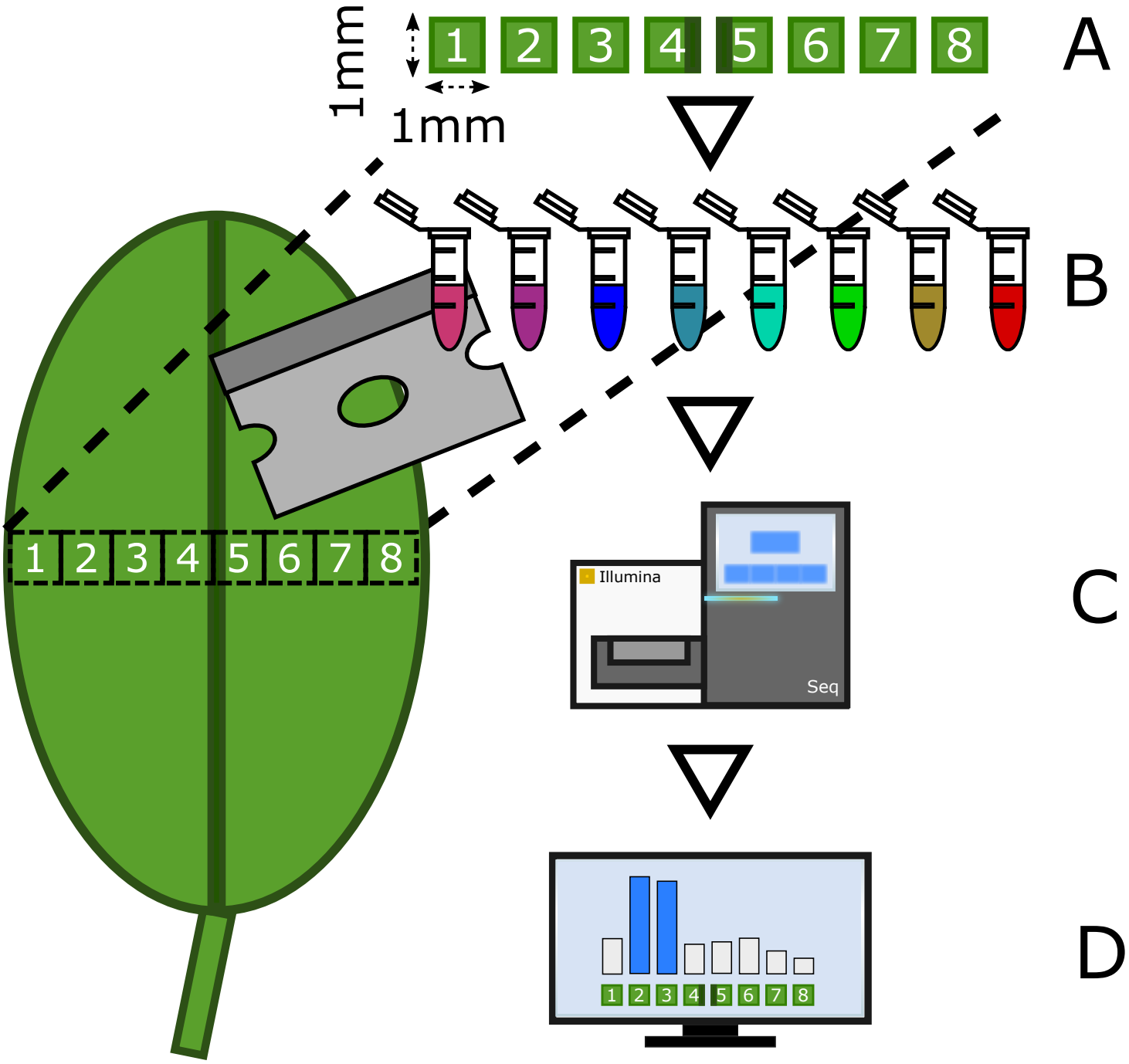
1mm
1mm
1 2 3 4 5 6 7 8
A
B
1 2 3 4 5 6 7 8
Illumina
Seq
C
1 2 3 4 5 6 7 8
D

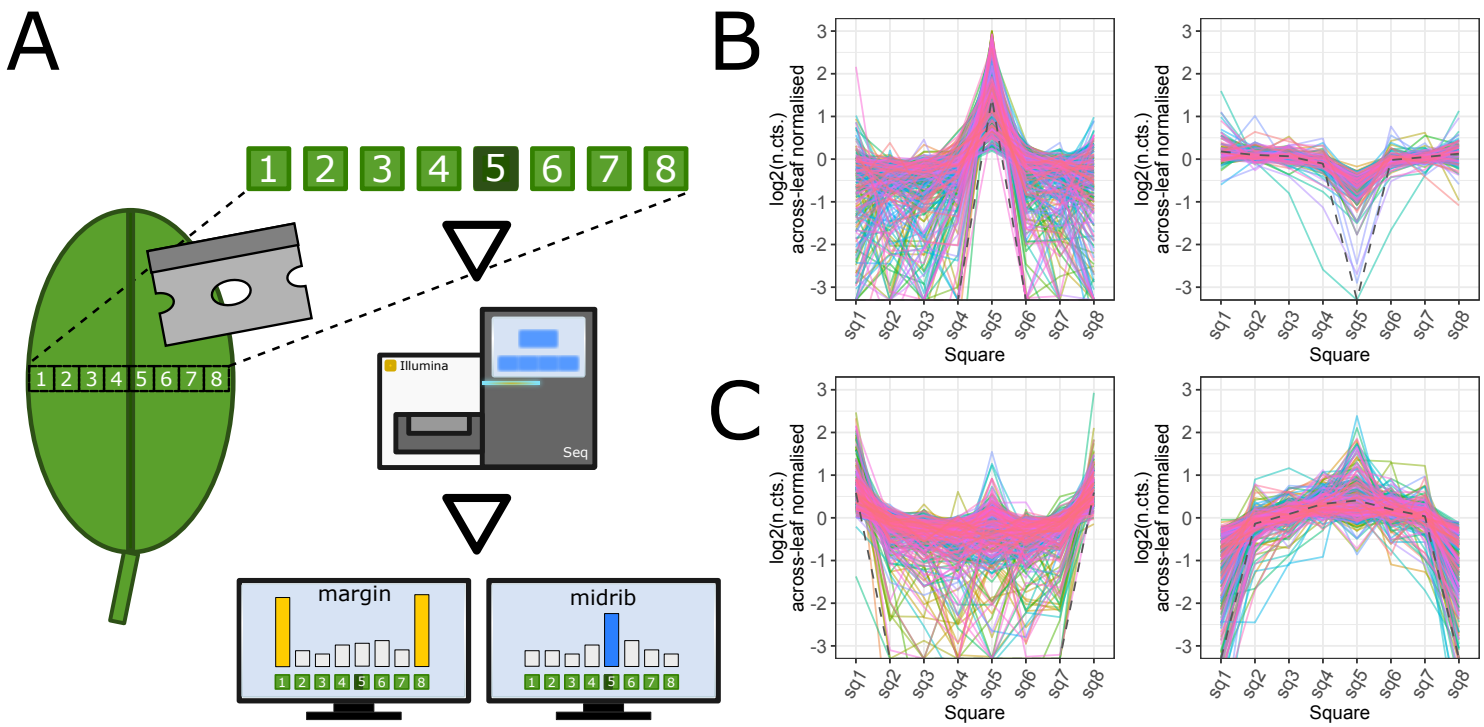
A
1 2 3 4 5 6 7 8
1 2 3 4 5 6 7 8
Illumina
Seq
margin
midrib
B
C
log2(n.cts.)
across-leaf normalised
Square
sq1
sq2
sq3
sq4
sq5
sq6
sq7
sq8

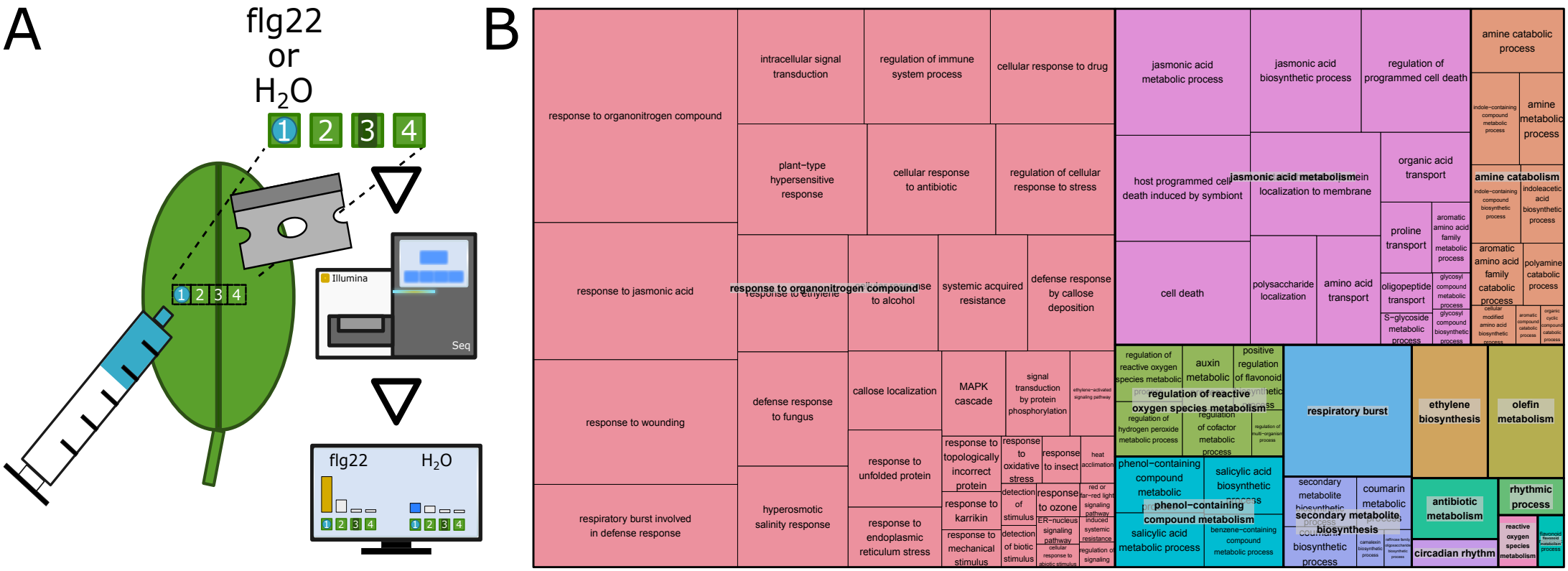
A
flg22
or
H_2O
1 2 3 4
1 2 3 4
Illumina
Seq
flg22
H_2O
1 2 3 4
1 2 3 4
B
response to organonitrogen compound
intracellular signal transduction
regulation of immune system process
cellular response to drug
plant−type hypersensitive response
cellular response to antibiotic
regulation of cellular response to stress
response to jasmonic acid
response to organonitrogen compound
response to ethylene
response to alcohol
systemic acquired resistance
defense response by callose deposition
response to wounding
defense response to fungus
callose localization
MAPK cascade
signal transduction by protein phosphorylation
ethylene−activated signaling pathway
response to unfolded protein
response to topologically incorrect protein
response to oxidative stress
response to insect
heat acclimation
response to karrikin
detection of stimulus
response to ozone
red or far−red light signaling pathway
ER−nucleus signaling pathway
induced systemic resistance
response to endoplasmic reticulum stress
response to mechanical stimulus
detection of biotic stimulus
cellular response to abiotic stimulus
regulation of signaling
respiratory burst involved in defense response
hyperosmotic salinity response
jasmonic acid metabolic process
jasmonic acid biosynthetic process
regulation of programmed cell death
host programmed cell death induced by symbiont
jasmonic acid metabolism
protein localization to membrane
organic acid transport
proline transport
aromatic amino acid family metabolic process
cell death
polysaccharide localization
amino acid transport
oligopeptide transport
glycosyl compound metabolic process
S−glycoside metabolic process
glycosyl compound biosynthetic process
amine catabolic process
indole−containing compound metabolic process
amine metabolic process
amine catabolism
indole−containing compound biosynthetic process
indoleacetic acid biosynthetic process
aromatic amino acid family catabolic process
polyamine catabolic process
cellular modified amino acid biosynthetic process
aromatic compound catabolic process
organic cyclic compound catabolic process
regulation of reactive oxygen species metabolic process
auxin metabolic process
positive regulation of flavonoid biosynthetic process
regulation of reactive oxygen species metabolism
regulation of hydrogen peroxide metabolic process
regulation of cofactor metabolic process
regulation of multi−organism process
respiratory burst
ethylene biosynthesis
olefin metabolism
phenol−containing compound metabolic process
salicylic acid biosynthetic process
phenol−containing compound metabolism
salicylic acid metabolic process
benzene−containing compound metabolic process
secondary metabolite biosynthetic process
coumarin metabolic process
secondary metabolite biosynthesis
coumarin biosynthetic process
camalexin biosynthetic process
raffinose family oligosaccharide biosynthetic process
antibiotic metabolism
rhythmic process
circadian rhythm
reactive oxygen species metabolism
flavonoid flavonoid metabolism process

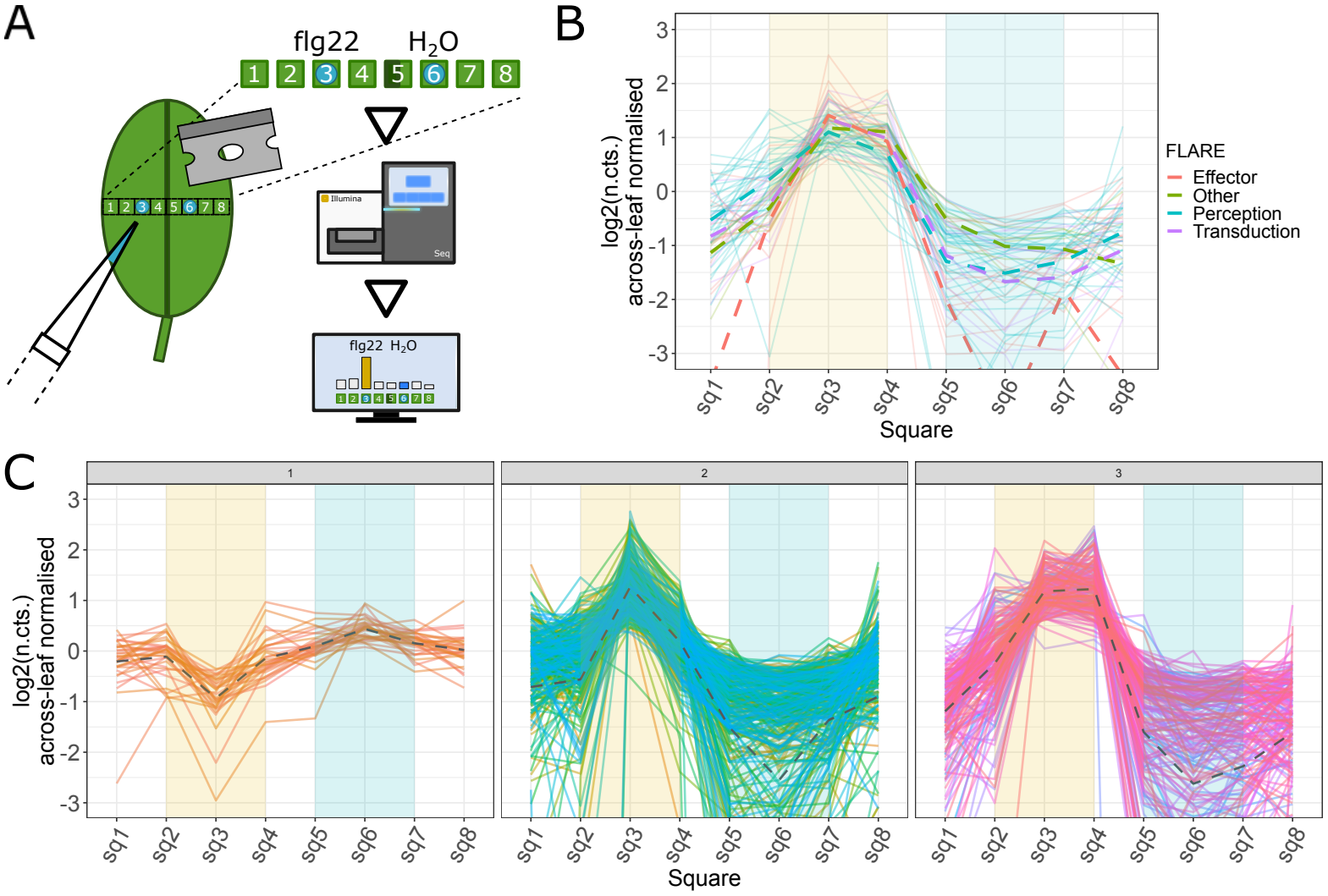
A
flg22
H_2O
1 2 3 4 5 6 7 8
Illumina
Seq
flg22 H_2O
B
log2(n.cts.)
across-leaf normalised
Square
sq1 sq2 sq3 sq4 sq5 sq6 sq7 sq8
FLARE
Effector
Other
Perception
Transduction
C
1
2
3
log2(n.cts.)
across-leaf normalised
Square

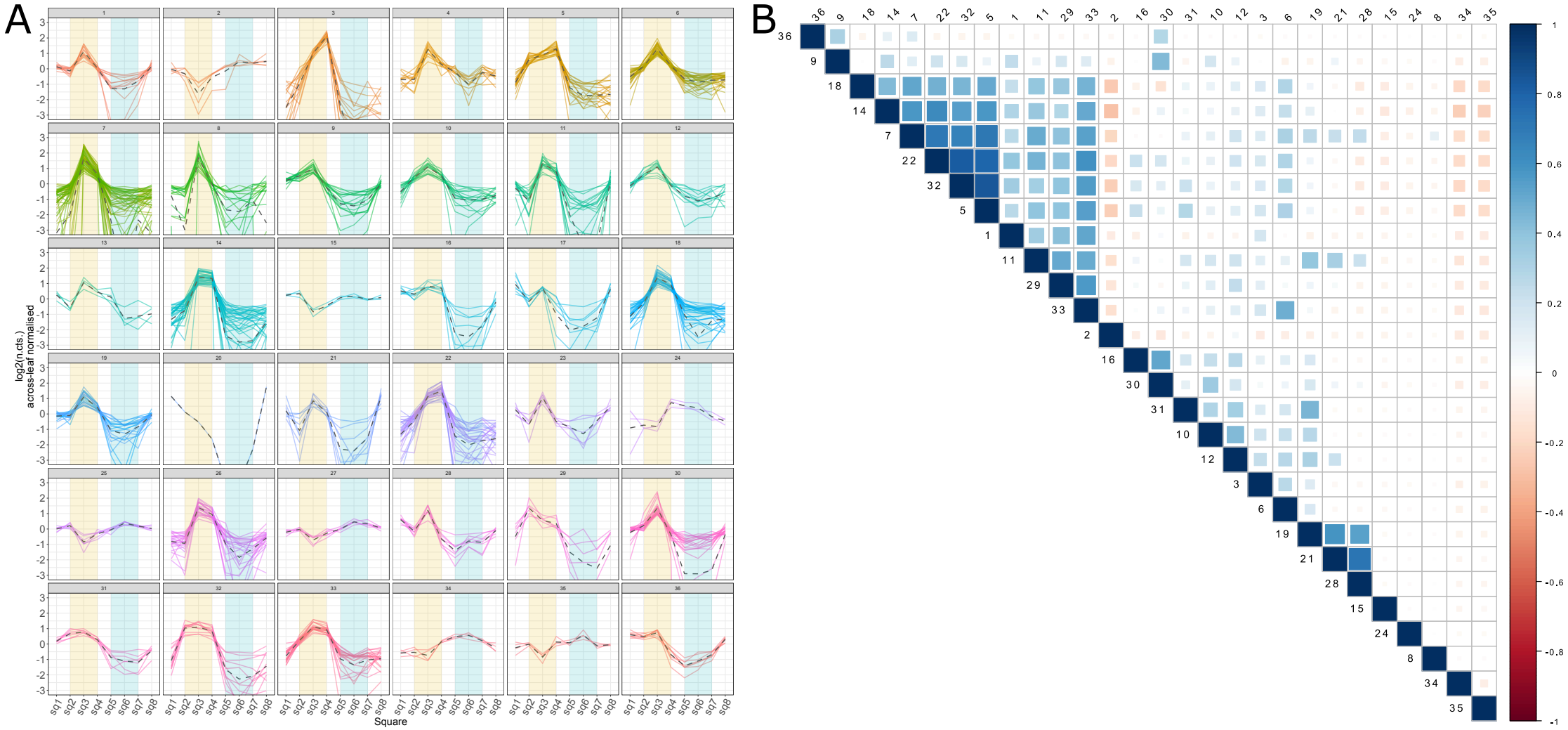
A
log2(n.cts.)
across-leaf normalised
Square
sq1
sq2
sq3
sq4
sq5
sq6
sq7
sq8
B
36
9
18
14
7
22
32
5
1
11
29
33
2
16
30
31
10
12
3
6
19
21
28
15
24
8
34
35
1
0.8
0.6
0.4
0.2
0
-0.2
-0.4
-0.6
-0.8
-1